

## REPORT 924

### APPLICATION OF THEODORSEN'S THEORY TO PROPELLER DESIGN

By JOHN L. CRIGLER

#### SUMMARY

*A theoretical analysis is presented for obtaining by use of Theodorsen's propeller theory the load distribution along a propeller radius to give the optimum propeller efficiency for any design condition. The efficiencies realized by designing for the optimum load distribution are given in graphs, and the optimum efficiency for any design condition may be read directly from the graph without any laborious calculations. Examples are included to illustrate the method of obtaining the optimum load distributions for both single-rotating and dual-rotating propellers.*

#### INTRODUCTION

Recent contributions to the theory of propellers have been made by Theodorsen in a series of reports (references 1 to 4). In the first report of the series (reference 1) a method based on electrical analogy was devised for obtaining the ideal circulation functions for single-rotating propellers. These circulation functions were shown to be in good agreement with the theoretical calculations made by Goldstein in reference 5 for two- and four-blade single-rotating propellers and with the extrapolations to other numbers of blades made by Lock and Yeatman in reference 6. The electrical-analogy method of measuring these functions was also applied to more difficult cases for which no theoretical calculations had previously been made; in particular, to the case of dual-rotating propellers.

Theodorsen in reference 1 introduced the concept of the mass coefficient  $\kappa$ , which is an integrated value of the circulation functions. The mass coefficient represents the effective cross section of the column of the medium pushed by the propeller divided by the projected-propeller-wake area.

This mass coefficient is made use of in the development of Theodorsen's theory. In reference 4, expressions are given for computing the thrust, the energy loss, and the efficiency of any propeller with ideal circulation distribution based on the conditions in the final wake in terms of the mass coefficient. It is of interest to mention that the mass coefficient or mass of air operated on by the dual-rotating propeller is much greater than that affected by the single-rotating propeller for the same set of operating conditions. This large difference in the mass coefficients for the two cases indicates that calculations for dual-rotating propellers based on the ideal circulation functions for single-rotating propellers are inadequate.

Theodorsen's theory, as previously mentioned, is based on the conditions in the final wake. The present analysis

attempts to interrelate the conditions in the final wake to the propeller and to give the information necessary to design a propeller for any desired operating condition. For single-rotating propellers, the method yields the same results as the conventional vortex theory with the Goldstein tip corrections applied. By the conventional vortex theory, however, it is necessary to determine the optimum blade-load distribution and then to make element strip-theory calculations in order to obtain the optimum efficiency for a given design condition. This procedure has been followed in reference 7 for a wide range of operating conditions. By Theodorsen's theory the optimum efficiency  $\eta$  can be obtained directly for any design condition from its relationship to the mass coefficient without laborious calculations. Thus, in the selection of a propeller for any design condition, a close estimate of the efficiency can be obtained before the design is made.

The circulation functions and mass coefficients for the dual-rotating propeller were obtained in reference 1 for the ideal case and refer to conditions in the ultimate wake. Both propellers were assumed to operate in the same plane. Obviously, this condition is unattainable in the design of an actual propeller. The degree to which the ideal case can be realized in practice, or the applicability of the ideal functions to a given case, require further consideration and confirmation.

#### SYMBOLS

$B$	number of propeller blades
$b$	chord of propeller-blade element
$c_d$	section drag coefficient
$c_l$	section lift coefficient
$P_c$	ideal power coefficient ( $c_s + e$ )
$P_{c_T}$	total-power coefficient ( $P_c + t_r$ )
$c_s$	thrust coefficient $\left( \frac{T}{\frac{1}{2} \rho V^2 F} \right)$
$c_{s_T}$	net thrust coefficient ( $c_s - t_a$ )
$D$	diameter of propeller
$d$	drag of propeller section
$D_0$	diameter of wake helix surface
$E$	ideal energy loss in wake $\left( \rho F \kappa w^2 \left( \frac{e}{\kappa} w + \frac{1}{2} V \right) \right)$
$E_D$	energy loss due to blade drag
$e$	induced energy loss coefficient $\left( \frac{E}{\frac{1}{2} \rho V^3 F} \right)$

$F$	projected area of helix (at infinity)
$K(x)$	circulation function
$l$	lift of propeller section
$n$	propeller rotational speed, revolutions per second
$P$	input power to propeller
$R$	tip radius
$r$	radius to any blade element
$T$	thrust of propeller
$t$	power loss due to drag (nondimensional)
$t_a$	axial power loss due to drag
$t_r$	rotational power loss due to drag
$V$	forward axial velocity of propeller
$V_a$	axial interference velocity (at propeller)
$\bar{V}_a$	average axial interference velocity (at propeller)
$V_t$	resultant interference velocity (at propeller)
$V_r$	rotational interference velocity (at propeller)
$\bar{V}_r$	average rotational interference velocity (behind each propeller)
$W$	resultant velocity on the propeller at radius $r$
$W_s$	local self-interference velocity
$w$	rearward displacement velocity of helical vortex surface
$\bar{w}$	ratio of displacement velocity to forward velocity ( $w/V$ )
$x$	radial location of blade element ( $r/R$ )
$\alpha$	angle of attack, degrees
$\alpha_t$	induced angle of attack, degrees
$\beta$	blade angle, degrees
$\lambda$	advance ratio $\left(\frac{1}{\pi} \frac{V+w}{nD_0}\right)$
$\lambda_s$	geometric advance ratio ( $V/\pi nD$ )
$\kappa$	mass coefficient $\left(2 \int_0^1 K(x) x dx\right)$
$\epsilon$	axial energy loss factor
$\eta$	propeller efficiency $\left(\frac{c_s - t_a}{P_c + t_r}\right)$
$\eta_i$	ideal propeller efficiency ( $c_s/P_c$ )
$\rho$	mass density of air
$\sigma$	propeller element solidity ( $Bb/2\pi r$ )
$\sigma c_i$	propeller element load coefficient
$\Gamma$	circulation at radius $x$ $\left(\Gamma(x) = \frac{2\pi(V+w)w}{B\omega} K(x)\right)$
$\phi$	angle of resultant velocity $W$ at plane of rotation
$\phi_0 = \tan^{-1} \frac{V/nD}{\pi x}$	
$\omega$	angular velocity
Subscripts:	
$F$	front
$R$	rear
$0.7R$	at 0.7 radius

## OPTIMUM PROPELLER DESIGN

## SINGLE-ROTATING PROPELLERS

**Velocity diagram.**—The velocity diagram for the single-rotating propeller is shown in figure 1. This figure is a reproduction of figure 13 (reference 2) with some additional designations. The relationship between the axial interference velocity at the radius  $r$ , as given by the vortex theory,

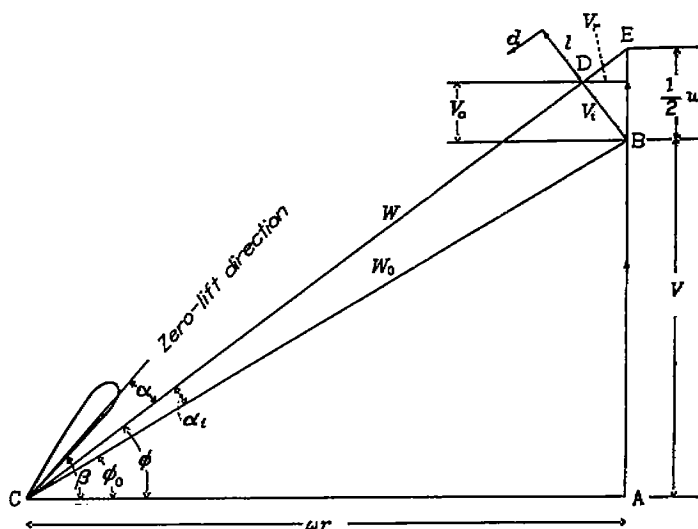


FIGURE 1.—Velocity diagram for single-rotating propeller.

to the displacement velocity  $w$  of the vortex sheet is calculated in reference 2 and is shown in figure 1. The forward axial velocity of the propeller is  $V$  and the tangential velocity with respect to the air at rest is  $\omega r$ . The vector  $BD$  is the resultant interference velocity  $V_t$  of the air with respect to the air at rest. Thus, the resultant velocity  $W$  of a point on the propeller at the radius  $r$  is given by the vector  $CD$ . The lift force  $l$  is perpendicular to this vector and the drag force  $d$  is exactly opposite in direction to  $W$  as indicated. From this figure a comparison of the method of analysis presented herein may be made with the conventional vortex-theory method. It is required to find the point  $D$  in order to locate the end of the velocity vector  $W$  and the angle  $\phi$  that the vector  $W$  makes with the direction of rotation. By the conventional vortex theory, the point  $D$  is located by starting with point  $B$  obtained from the  $V/nD$  of the undisturbed flow, proceeding in the  $V$ -direction the distance  $V_a$ , and then taking the perpendicular to this direction a distance  $V_r$ . (See reference 8.) The angle  $\phi$  is given by  $\tan \phi = \frac{V+V_a}{\omega r - V_r}$  and  $W = \frac{V+V_a}{\sin \phi}$ . In the calculation of interference velocities  $V_a$  and  $V_r$ , the local tip correction or Goldstein factor must be used to obtain the correct location of the point  $D$ .

With the method developed in references 1 to 4, only the value of  $\frac{1}{2}w$ , which remains constant with radius, need be used. With this concept it is possible to use the integrated values of the mass coefficient as determined by the electrical analogy of reference 1 to obtain the detailed information needed at any radius. By this method the point  $D$  can be located by proceeding from point  $B$  a distance  $\frac{1}{2}w$  in the  $V$ -direction to the point  $E$  and then down the direction of the velocity vector  $W$  a distance  $DE$ , where  $DE$  is obtained from the geometry of the figure as  $\frac{1}{2}w \sin \phi$  and

$$\tan \phi = \frac{V + \frac{1}{2}w}{\omega r} \quad (1)$$

The resultant velocity is

$$\begin{aligned} W &= \frac{V + \frac{1}{2}w}{\sin \phi} - \frac{1}{2}w \sin \phi \\ &= \frac{1}{\sin \phi} \left( V + \frac{1}{2}w \cos^2 \phi \right) \end{aligned} \quad (2)$$

The interference velocities may be obtained from the geometry of the figure by

$$V_t = \frac{1}{2}w \cos \phi$$

$$V_s = V_t \cos \phi = \frac{1}{2}w \cos^2 \phi$$

and

$$V_r = V_t \sin \phi = \frac{1}{2}w \sin \phi \cos \phi$$

**Optimum blade-load distribution.**—The design problem of an optimum propeller consists essentially in obtaining the value of the element load coefficient  $bc_i$  at each radius of the propeller blade. With the direction and magnitude of the relative velocity given at each station there remains only the choice of a section to give efficiently such a lift at the appropriate angle of attack. The value of  $c_i$  should be at or near the ideal lift coefficient for the section in order to give minimum drag coefficient.

The method developed in references 1 to 4 treats the velocity  $w$  as an independent parameter upon which all the other quantities depend. This reversal of procedure is convenient since all quantities are actually functions of  $w$ . The velocity  $w$  is related to the power coefficient  $P_e$  of the propeller and also to the element load coefficient  $\sigma c_i$ . The relation of  $w$  to  $\sigma c_i$  is developed herein and the relation of  $w$  to  $P_e$ , which must be obtained in order to use it for design, is given subsequently in the section "Procedure for Propeller Design."

The required ideal circulation  $\Gamma(x)$  is given in reference 1 by

$$\begin{aligned} \Gamma(x) &= \frac{2\pi(V+w)w}{Bw} K(x) \\ &= \frac{(V+w)w}{Bn} K(x) \end{aligned} \quad (3)$$

In order to determine the element load coefficient  $bc_i$ , the relation for the equality of the force on a vortex element and on an element of a lifting surface is given as

$$\rho \Gamma W = \frac{1}{2} \rho W^2 c_i b$$

where  $b$  is the chord of the element. Hence,

$$\Gamma = \frac{1}{2} W c_i b \quad (4)$$

where  $W$  is given in equation (2), and thus

$$\Gamma = \frac{1}{2} \frac{1}{\sin \phi} \left( V + \frac{1}{2}w \cos^2 \phi \right) c_i b \quad (5)$$

Using equations (3) and (5) for  $\Gamma$  gives at once the identity

$$bc_i = \frac{(V+w)w}{Bn} K(x) \frac{2 \sin \phi}{V + \frac{1}{2}w \cos^2 \phi}$$

Introducing the nondimensional velocity  $\bar{w} = \frac{w}{V}$ , the

solidity  $\sigma = \frac{Bb}{2\pi r}$ , and  $\tan \phi = \frac{V + \frac{1}{2}w}{2\pi r n}$  (equation (1)) gives the

nondimensional relation

$$\sigma c_i = \frac{1 + \bar{w}}{\left(1 + \frac{1}{2}\bar{w}\right) \left(1 + \frac{1}{2}\bar{w} \cos^2 \phi\right)} 2\bar{w} K(x) \frac{\sin^2 \phi}{\cos \phi} \quad (6)$$

The selection of a propeller for a given airplane installation may be based on a method of evaluating a series of propellers for various operating conditions in order to determine the most suitable propeller. It is probable that several propellers, varying in diameter, blade number, propeller operational speed, and direction of rotation are equally as efficient for the design condition so that other considerations may enter into the propeller selection. However, the optimum efficiency for the propeller selected may be obtained from the charts, and therefore the load distribution along the radius that will give this optimum efficiency remains to be determined.

The value of  $\sigma c_i$  may be calculated for any radius from the relation

$$\sigma c_i = \frac{1 + \bar{w}}{\left(1 + \frac{1}{2}\bar{w}\right) \left(1 + \frac{1}{2}\bar{w} \cos^2 \phi\right)} 2\bar{w} K(x) \frac{\sin^2 \phi}{\cos \phi}$$

where

$$\phi = \tan^{-1} \frac{1}{\pi n D} \frac{V + \frac{1}{2}w}{x} = \tan^{-1} \lambda_r \frac{1 + \frac{1}{2}\bar{w}}{x} \quad (7)$$

#### DUAL-ROTATING PROPELLERS

In the design of dual-rotating propellers, it has been customary to select two propellers designed for single rotation and to use them as a dual-rotating propeller. The fact that the circulation functions and the mass coefficients obtained by the electrical-analogy method (reference 1) are very much larger for the dual-rotating propeller than the sum of the values for the two single-rotating propellers indicates that the functions as used heretofore are not proper. The electrical-analogy method represents the case of an idealized dual-rotating propeller in which the two components are in the same plane with the same load distribution on each component and with equal power absorption. Since actual propellers cannot conform to this ideal case, the applicability of the ideal functions requires further confirmation. Nevertheless, the optimum distribution for the dual-rotating propeller is essentially different from the single-rotating propeller, and in this analysis the loading functions and the mass coefficients as determined by the electrical-analogy method are assumed to apply to the optimum dual-rotating propeller.

**Interference velocities for dual-rotating propellers.**—The average axial interference velocity far behind the propeller obtained from the momentum considerations is

$$2\bar{V}_a = \kappa w$$

where  $\kappa$  is the mass coefficient and  $w$  is the axial displacement velocity. This mean value is equally due to each of the two oppositely rotating propellers. The average axial interference velocity due to each is therefore exactly

$$\bar{V}_a = \frac{1}{2} \kappa w$$

The average interference velocity at the propeller plane is one-half the value in the final wake and, therefore,

$$\frac{1}{2} \bar{V}_a = \frac{1}{4} \kappa w$$

where  $\frac{1}{2} \bar{V}_a$  represents the average axial interference velocity at the propeller plane due to each component of the dual-rotating propeller. With the two propellers separated by a small axial distance, this velocity refers to a plane between the two propellers. The interference velocity at the front propeller is smaller and at the rear propeller is larger than at the plane between the propellers. In the following treatment, the propellers are considered to be very close together so that the axial interference velocity is the same on both propellers.

In the final wake, the mean value of the rotational interference velocity for the ideal case is given by

$$2\bar{V}_r = 0$$

For an infinite number of right and left blades equally loaded, rotational components would cancel exactly. However, the average rotational interference velocity immediately behind each propeller may be considered as

$$\bar{V}_r = \frac{1}{2} \kappa w \tan \phi$$

In summary, the mean interference velocities acting on the front propeller from the rear propeller are

Axial:

$$\frac{1}{2} \bar{V}_a = \frac{1}{4} \kappa w$$

Rotational:

$$\bar{V}_r = 0$$

The mean interference velocities acting on the rear propeller from the front propeller are

Axial:

$$\frac{1}{2} \bar{V}_a = \frac{1}{4} \kappa w$$

Rotational:

$$\bar{V}_r = \frac{1}{2} \kappa w \tan \phi$$

It is useful to recognize that the mean self-interference of each propeller in its own plane is

Axial:

$$\frac{1}{4} \kappa w$$

Rotational:

$$\frac{1}{4} \kappa w \tan \phi$$

**Velocity diagram for the dual-rotating propellers.**—The velocity diagram for the dual-rotating propellers is shown in figure 2. As in the case for the single-rotating propeller, the axial displacement velocity at the propeller is equal to  $\frac{1}{2} w$ . In figure 2 the vector AB gives the mean axial interference velocity  $\frac{1}{4} \kappa w$  of each propeller acting on the other propeller. The vector BC gives the mean rotational interference velocity  $\frac{1}{2} \kappa w \tan \phi$  of the front propeller acting on the rear propeller. The total interference velocity acting on the front propeller from the rear propeller is therefore given by AC, and the total interference velocity acting on the rear propeller from the front propeller is equal to the vector AE. The local self-interference velocity of the front propeller is given by  $W_{SF}$ , and the corresponding helix angle is given by  $\phi_F$ . The local self-interference velocity of the rear propeller is given by  $W_{SR}$ , and the corresponding helix angle is given by  $\phi_R$ . The angle  $\phi_F$  is slightly larger than the ideal helix angle  $\phi$  given by the displacement velocity  $\frac{1}{2} w$  and  $\phi_R$  is slightly smaller than  $\phi$ . The design condition of most interest is the one for which  $\Gamma_F$  for each blade of the front propeller is equal to  $\Gamma_R$  for each blade of the rear propeller. The number of blades on the front and rear

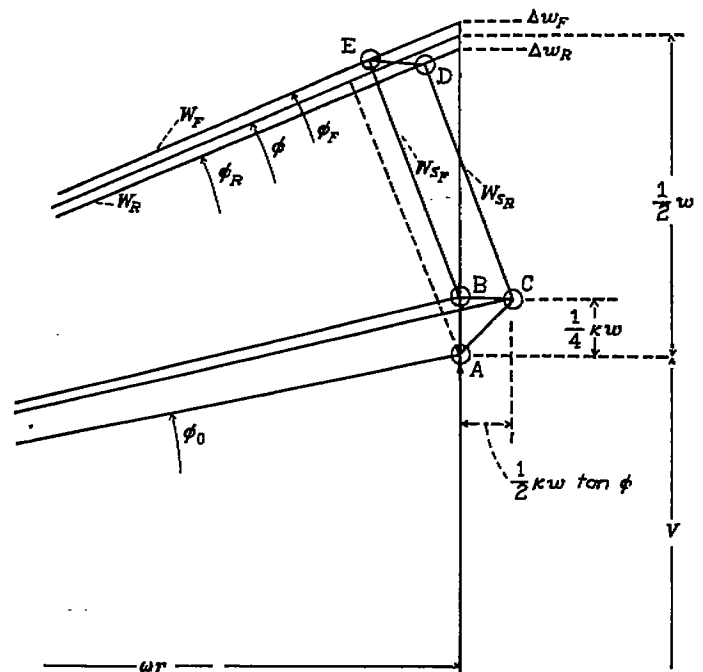


FIGURE 2.—Velocity diagram for dual-rotating propeller.

propeller are considered equal and the rotational speeds, the same. This condition gives the self-interference velocity on the front propeller equal to the self-interference velocity on the rear propeller and means that D and E must be at the same horizontal level.

As  $\phi_F$  and  $\phi_E$  are needed in the design of the propeller, it is seen from figure 2 that the associated displacement velocity on the front and rear propellers has been increased and decreased, respectively, by the amount

$$\Delta w = \frac{1}{4} \kappa w \tan^2 \phi$$

The displacement velocity is therefore

Front:

$$\frac{1}{2} w \left( 1 + \frac{1}{2} \kappa \tan^2 \phi \right)$$

Rear:

$$\frac{1}{2} w \left( 1 - \frac{1}{2} \kappa \tan^2 \phi \right)$$

From figure 2, the velocity  $W_F$  is shown to be given by the relationship

$$\begin{aligned} W_F &= \frac{V}{\sin \phi_0} + \frac{1}{4} \kappa w \sin \phi_0 \\ &= \frac{V}{\sin \phi_0} \left( 1 + \frac{1}{4} \kappa \bar{w} \sin^2 \phi_0 \right) \end{aligned} \quad (8)$$

and the angle  $\phi_F$  is given by

$$\begin{aligned} \tan \phi_F &= \frac{V + \frac{1}{2} w \left( 1 + \frac{1}{2} \kappa \tan^2 \phi \right)}{\omega r} \\ &= \frac{V}{nD} \frac{1}{\pi x} \left[ 1 + \frac{1}{2} \bar{w} \left( 1 + \frac{1}{2} \kappa \tan^2 \phi \right) \right] \end{aligned} \quad (9)$$

where  $\phi$  is given by the relationship

$$\begin{aligned} \tan \phi &= \frac{V + \frac{1}{2} w}{\omega r} \\ &= \frac{V}{nD} \frac{1}{\pi x} \left( 1 + \frac{1}{2} \bar{w} \right) \end{aligned}$$

Similarly,

$$\begin{aligned} W_E &= \frac{V}{\sin \phi_0} + \frac{1}{4} \kappa w \sin \phi_0 + \frac{1}{2} \kappa w \tan \phi_0 \cos \phi_0 \\ &= \frac{V}{\sin \phi_0} + \frac{3}{4} \kappa w \sin \phi_0 \\ &= \frac{V}{\sin \phi_0} \left( 1 + \frac{3}{4} \kappa \bar{w} \sin^2 \phi_0 \right) \end{aligned} \quad (10)$$

and

$$\begin{aligned} \tan \phi_E &= \frac{V + \frac{1}{2} w \left( 1 - \frac{1}{2} \kappa \tan^2 \phi \right)}{\omega r} \\ &= \frac{V}{nD} \frac{1}{\pi x} \left[ 1 + \frac{1}{2} \bar{w} \left( 1 - \frac{1}{2} \kappa \tan^2 \phi \right) \right] \end{aligned} \quad (11)$$

**Optimum blade-load distribution.**—The optimum distribution of blade loading is obtained from the determination of the element load coefficient  $bc_i$  at each radius from the fundamental relation

$$\frac{1}{2} \rho bc_i W^2 = \rho \Gamma W$$

where  $\Gamma$  has been given in equation (3) by

$$\Gamma = \frac{(V+w)w}{Bn} K(x)$$

Eliminating  $\Gamma$  gives

$$\frac{1}{2} Bbc_i W = \frac{(V+w)w}{n} K(x)$$

but  $\frac{1}{2} \frac{Bb}{2\pi r} = \sigma$  is the solidity of each component of the dual-rotating propeller, if the number of blades in each component are assumed to be equal. Therefore,

$$\sigma c_i W = \frac{V}{\pi n D x} (1 + \bar{w}) \bar{w} V K(x)$$

For the front propeller, this equation may be solved by use of equation (8)

$$(\sigma c_i)_F = \frac{V}{nD} \frac{1}{\pi x} \frac{(1 + \bar{w}) \bar{w} \sin \phi_0}{1 + \frac{1}{4} \kappa \bar{w} \sin^2 \phi_0} K(x) \quad (12)$$

and for the rear propeller by use of equation (10)

$$(\sigma c_i)_E = \frac{V}{nD} \frac{1}{\pi x} \frac{(1 + \bar{w}) \bar{w} \sin \phi_0}{1 + \frac{3}{4} \kappa \bar{w} \sin^2 \phi_0} K(x) \quad (13)$$

#### USE OF DESIGN FORMULAS

In order to use the relation for  $\sigma c_i$ , note that it contains not only the independent variable  $\bar{w}$  but also the function  $K(x)$  and the angle  $\phi$ . The parameter  $K(x)$  should be expressed as a function of  $\frac{V+w}{nD_0}$ , which is based on the wake helix diameter. As was shown in reference 3, however,  $D_0$  differs only slightly from the propeller diameter  $D$  and in the present design procedure  $D$  is used instead of  $D_0$ . The function  $K(x)$  for single-rotating propellers is plotted against  $\frac{V+w}{nD}$  in figure 3. Similar plots for dual-rotating propellers were taken from reference 1 and are presented in figure 4.

#### EQUATIONS FOR PERFORMANCE CALCULATIONS

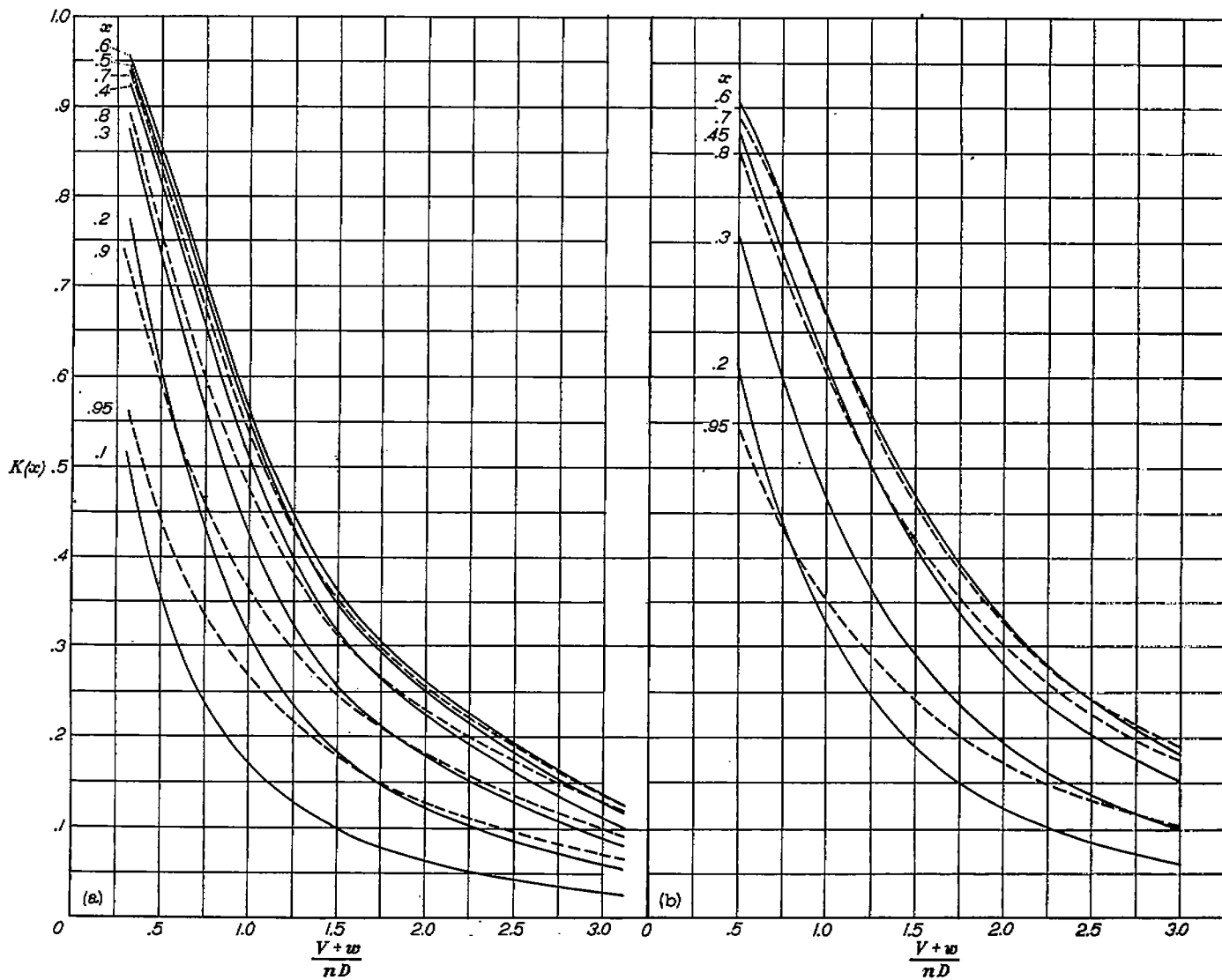
##### SINGLE-ROTATING PROPELLERS

In reference 4 the thrust has been given by

$$T = \rho F \kappa w \left[ V + w \left( \frac{1}{2} + \frac{\epsilon}{\kappa} \right) \right]$$

and the ideal energy loss in the wake has been given by

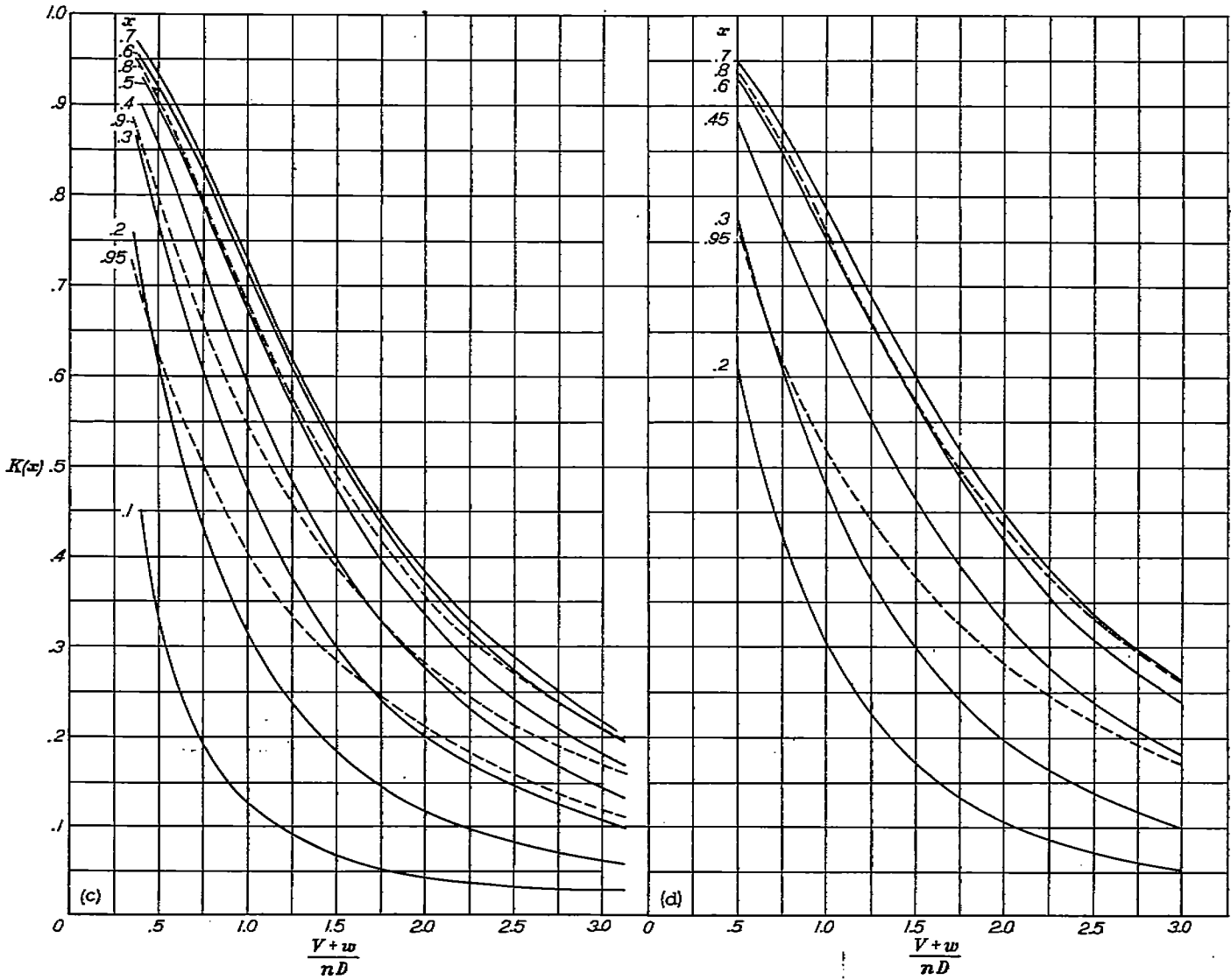
$$E = \rho F \kappa w^2 \left( \frac{\epsilon}{\kappa} w + \frac{1}{2} V \right)$$



(a) Two-blade single-rotating propeller (reference 6).

(b) Three-blade single-rotating propeller (reference 6).

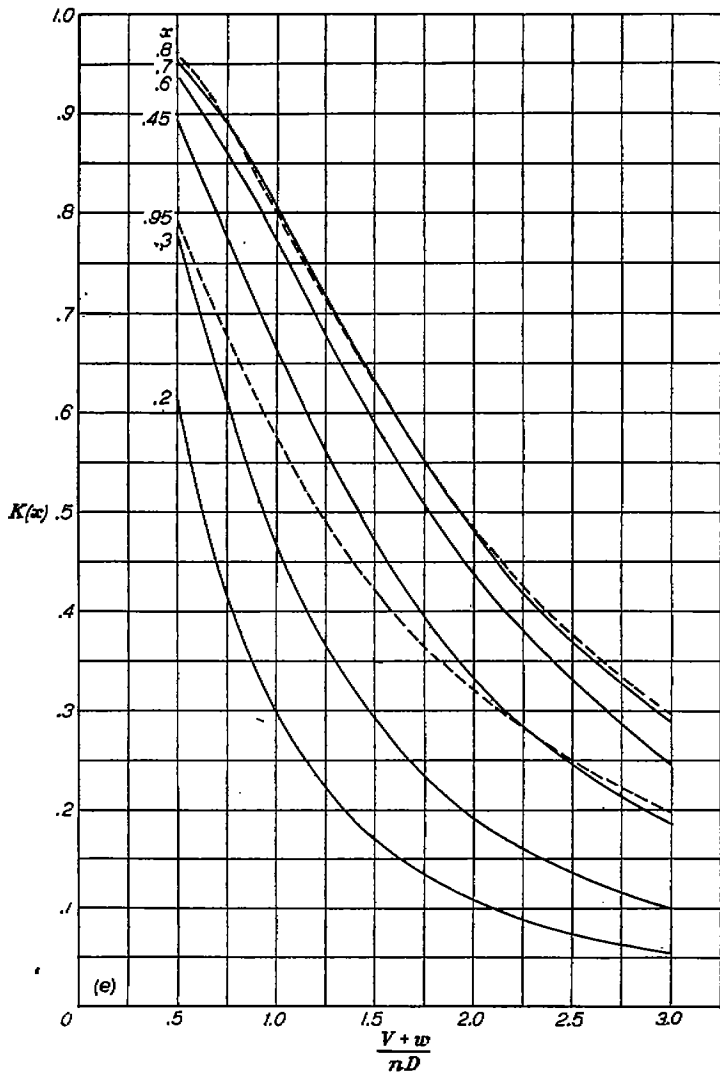
FIGURE 3.—Circulation function  $K(x)$  for single-rotating propellers.



(c) Four-blade single-rotating propeller.

(d) Six-blade single-rotating propeller.

FIGURE 3.—Continued.



(e) Eight-blade single-rotating propeller.

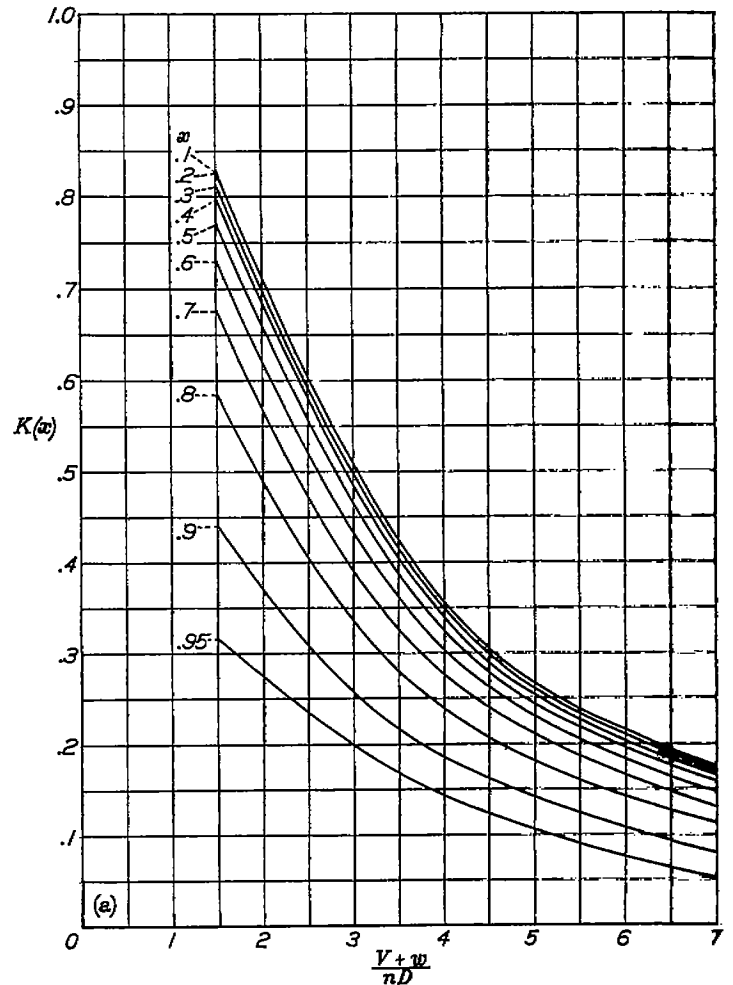
FIGURE 3.—Concluded.

With the introduction of the nondimensional quantity  $\bar{w} = \frac{w}{V}$ , the thrust coefficient in nondimensional form is

$$c_s = \frac{T}{\frac{1}{2} \rho V^2 F} = 2\kappa \bar{w} \left[ 1 + \bar{w} \left( \frac{1}{2} + \frac{\epsilon}{\kappa} \right) \right] \quad (14)$$

and the induced loss coefficient is

$$e = \frac{E}{\frac{1}{2} \rho V^3 F} = 2\kappa \bar{w}^2 \left( \frac{1}{2} + \frac{\epsilon}{\kappa} \bar{w} \right) \quad (15)$$



(a) Four-blade dual-rotating propeller.

FIGURE 4.—Circulation function  $K(x)$  for dual-rotating propellers (reference 1).

The power coefficient  $P_c = c_s + e$  is given by

$$P_c = 2\kappa \bar{w} (1 + \bar{w}) \left( 1 + \frac{\epsilon}{\kappa} \bar{w} \right) \quad (16)$$

The efficiency is given by

$$\eta_i = \frac{c_s}{P_c} \quad (17)$$

These formulas are all that are necessary for single-rotating propellers. The performance of the dual-rotating propeller is computed by the same formulas.

DUAL-ROTATING PROPELLERS

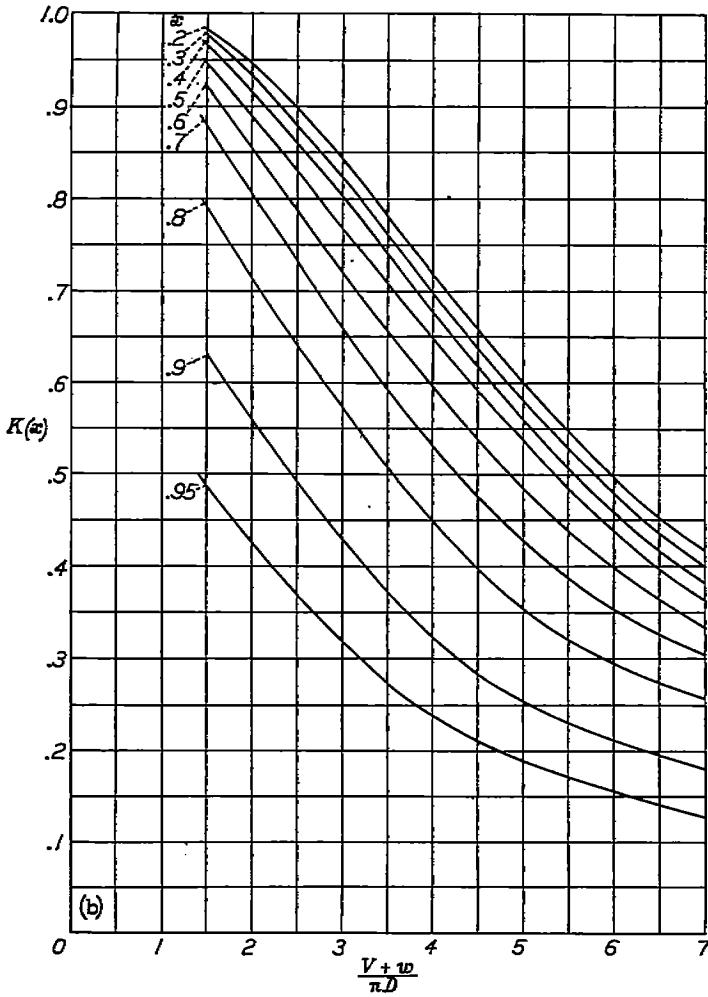
The thrust of the front propeller is given by

$$dT_F = \frac{1}{2} \rho (2\pi r) W_F^2 (\sigma c_i)_F \cos \phi_F dr$$

and with  $(\sigma c_i)_F$  from equation (12) and  $W_F$  from equation (8)

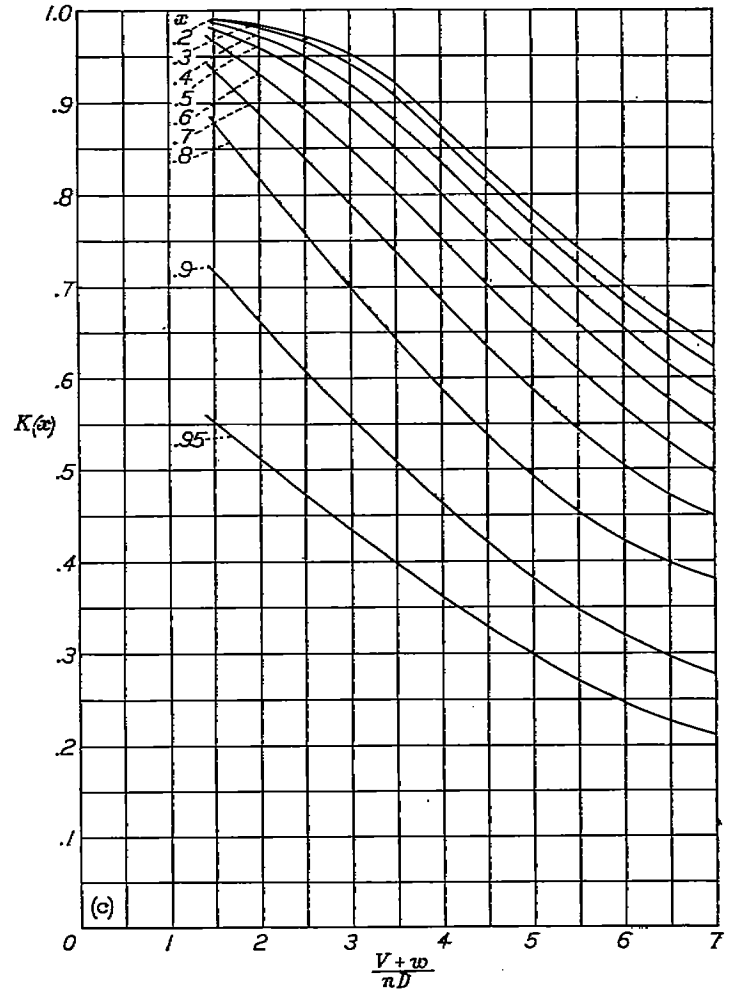
$$T_F = \rho \frac{D}{4} V^3 \bar{w} (1 + \bar{w}) \frac{1}{n} \int_0^1 \left( 1 + \frac{1}{4} \kappa \bar{w} \sin^2 \phi_0 \right) \frac{\cos \phi_F}{\sin \phi_0} K(x) dx \quad (18)$$





(b) Eight-blade dual-rotating propeller.

FIGURE 4.—Continued.



(c) Twelve-blade dual-rotating propeller.

FIGURE 4.—Concluded.

Similarly, for the rear propeller

$$T_R = \rho \frac{D}{4} V^3 \bar{w} (1 + \bar{w}) \frac{1}{n} \int_0^1 \left( 1 + \frac{3}{4} \kappa \bar{w} \sin^2 \phi_0 \right) \frac{\cos \phi_R}{\sin \phi_0} K(x) dx \quad (19)$$

The coefficients  $c_s$ ,  $e$ , and  $P_c$  for the dual-rotating propellers are given in the same form as in equations (14), (15), and (16) for single-rotating propellers. The only difference in the coefficients results from differences in the values of  $\kappa$ ,  $\bar{w}$ , and  $\epsilon/\kappa$  which are substituted in the equations.

BLADE-DRAG LOSSES

The frictional loss or loss in efficiency due to the profile drag of the blade is

$$E_D = B \frac{\rho}{2} \int_0^R bc_s W^3 dr$$

The drag force per unit length is  $\frac{1}{2} \rho W^2 bc_s$  where  $W$ , the resultant velocity of the blade element, has been given in

equation (2) for single-rotating propellers by

$$W = \frac{1}{\sin \phi} \left( V + \frac{1}{2} w \cos^2 \phi \right)$$

For the design condition,  $w$  is small, and because of the obvious uncertainties in the determination of the value of  $c_s$ , it is not necessary to retain the second term  $\frac{1}{2} w \cos^2 \phi$ . Introducing the solidity factor  $\sigma = \frac{Bb}{2\pi r}$  permits the drag loss to be given by

$$E_D = \pi R^2 \rho V^3 \int_0^1 \frac{\sigma c_s}{\sin^3 \phi} x dx$$

or in nondimensional form

$$\begin{aligned} i &= \frac{E_D}{\frac{1}{2} \rho V^3 \pi R^2} \\ &= 2 \int_0^1 \frac{\sigma c_s}{\sin^3 \phi} x dx \end{aligned} \quad (20)$$

The component power losses are then, to the same degree of approximation in nondimensional form,

Rotational:

$$t_r = \frac{2}{\lambda_\epsilon^2} \int_0^1 \frac{\sigma c_d}{\sin \phi} x^3 dx \quad (21)$$

Axial:

$$t_a = 2 \int_0^1 \frac{\sigma c_d}{\sin \phi} x dx \quad (22)$$

For the dual-rotating propeller operating at the design conditions, the terms containing  $w$  are small, as is the case with the single-rotating propeller, and a close approximation to the drag loss is obtained if these terms are neglected. Furthermore, if it is assumed that the average of the resultant velocity  $W$  for the dual combination is equal to  $W$  for the single propeller, equations (20) to (22) may be used for the dual-rotating propellers. Of course, for conditions other than the design condition, especially for very heavy loadings, exact drag-loss calculations require that the exact equations be used for either single-rotating or dual-rotating propellers.

In summary, the equations for obtaining the propeller performance are given by the quantities  $c_s$ ,  $e$ , and  $P_c$  and the drag-loss factors are given by  $t_r$  and  $t_a$ .

The net thrust power is

$$c_{sT} = c_s - t_a \quad (23)$$

The power input is

$$P_{cT} = c_s + e + t_r = P_c + t_r \quad (24)$$

The efficiency is

$$\eta = \frac{c_s - t_a}{P_c + t_r} = \frac{c_{sT}}{P_{cT}} \quad (25)$$

where from equation (16)

$$P_c = 2\kappa\bar{w}(1+\bar{w}) \left(1 + \frac{\epsilon}{\kappa}\bar{w}\right)$$

The total power is also given by

$$P = \frac{1}{2} \rho V^3 \pi R^2 P_{cT} \quad (26)$$

It should be remembered that the calculation is based on a given  $\bar{w}$ . This procedure may seem unjustifiable since this parameter is not given by the specification but is the end result of a calculation based on the original data. The induced loss does not depend on the total-power coefficient  $P_{cT}$  but actually depends only on  $P_c$ , and the quantity  $\bar{w}$  cannot be obtained from the total-power coefficient. However, the value of  $P_{cT}$  in most cases exceeds  $P_c$  by not more than 2 percent or

$$P_{cT} = 0.98 P_c$$

Since  $P_c$  in equation (16) is based on  $\bar{w}$  and the diameter of the final wake and since the value of  $P_{cT}$  in equation (24) is based on the propeller diameter which is slightly larger than the diameter of the final wake, a very close approximation to  $\bar{w}$  is usually given by equation (16). Therefore,

$$P_{cT} \approx P_c = 2\kappa\bar{w}(1+\bar{w}) \left(1 + \frac{\epsilon}{\kappa}\bar{w}\right)$$

In some cases it may be necessary to calculate  $t_r$  to obtain a more exact value of  $P_c$ , especially if the blade profile drag is large.

## PROCEDURE FOR DESIGN OF PROPELLER

### FIGURES USED IN PROPELLER DESIGN

The information necessary to design a propeller for any operating condition is given in the figures. Figure 3 gives the circulation function  $K(x)$  interpolated for even fractions for 2-, 3-, 4-, 6-, and 8-blade single-rotating propellers. The circulation function for the 2-blade propeller was taken directly from reference 5; for the 3-blade propeller, from reference 6; and for the propellers having a greater number of blades was recalculated from the Goldstein tip correction factors as given in reference 7. Figure 4 gives  $K(x)$  for dual-rotating propellers with 4, 8, and 12 blades. These values for the dual-rotating propellers were taken from data of reference 1. Figure 5 gives the mass coefficient  $\kappa$  for various numbers of blades for single-rotating propellers. Figure 6, which was taken from reference 1, gives  $\kappa$  for dual-rotating propellers. The ideal efficiency  $\eta_i$  is plotted against  $\bar{w}$  for a range of values  $\epsilon/\kappa$  in figure 7, against  $c_s/\kappa$  in figure 8, and against  $P_c/\kappa$  in figure 9. The data for figures 7 and 8 were taken directly from reference 4 and the data for figure 9 were recalculated by the use of equation (16) and figure 7. Figures 7 to 9 apply to either single- or dual-rotating propellers. The propeller efficiency may be calculated from either of these figures; however, in this report the efficiency has been determined from  $P_c/\kappa$  as given in figure 9.

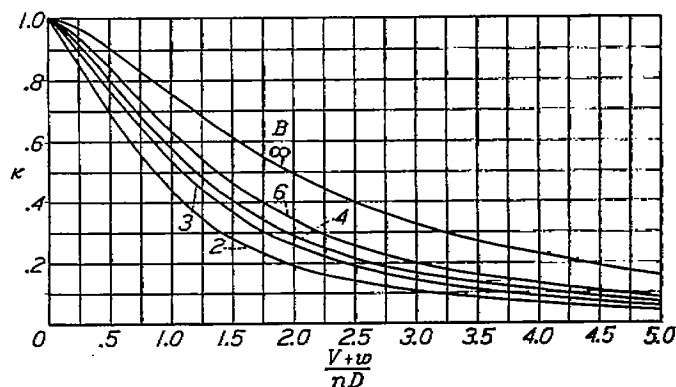


FIGURE 5.—Mass coefficient  $\kappa$  against  $\frac{V+w}{nD}$  for various numbers of blades for single-rotating propellers.

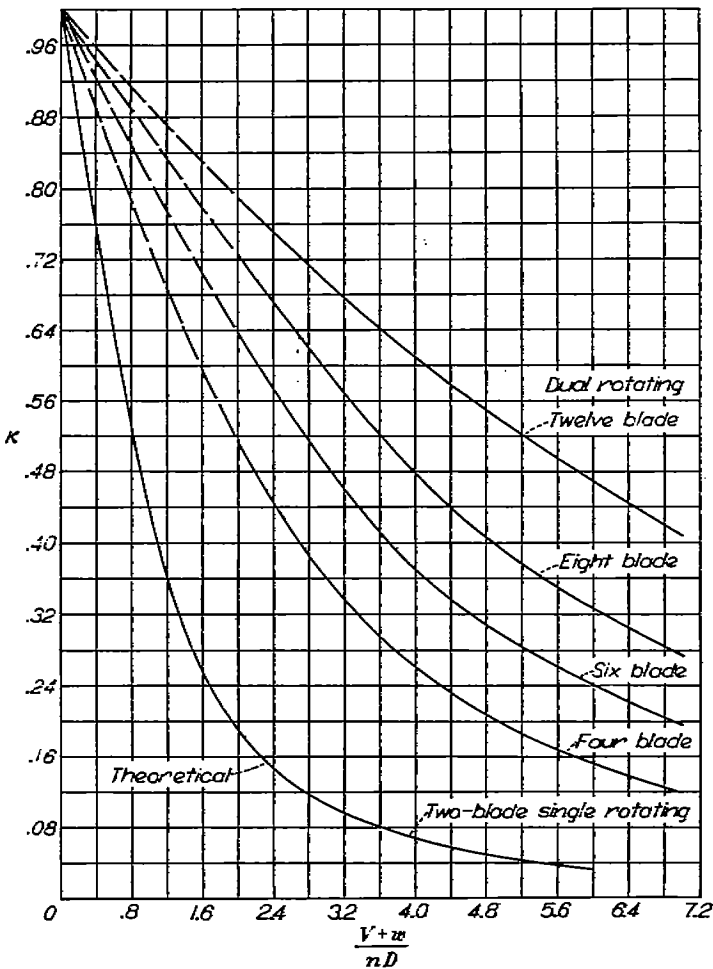


FIGURE 6.—Measured values of mass coefficient  $\kappa$  for dual-rotating propellers with various numbers of blades. Two-blade single-rotating propeller included for comparison (reference 1).

Figure 10 gives values of  $\epsilon$ ,  $\kappa$ , and  $\epsilon/\kappa$  for 2- and 4-blade single-rotating propellers and figure 11 gives values for 4-, 8-, and 12-blade dual-rotating propellers. The values of  $\epsilon$  for a propeller with a finite number of blades have not previously been published, but the values of  $\epsilon$  and  $\epsilon/\kappa$  for an infinite number of blades are given in figure 4 of reference 4. The method for calculating  $\epsilon/\kappa$  and  $\epsilon$  is given in the following section.

PROPELLER SELECTION

In the selection of a propeller for a given airplane installation, the engine power, the forward speed, and the design altitude are usually specified. The selection consists of the determination of the number of blades, the propeller solidity, the propeller diameter, and the rotative speed. The ideal propeller efficiency for any combinations of these variables can be readily obtained with the use of the charts. The procedure for a given blade number, propeller diameter, and rotative speed for either single or dual rotation is as follows:

First, calculate the total-power coefficient

$$P_{c_T} = \frac{P}{\frac{1}{2} \rho V^3 \frac{\pi}{4} D^2}$$

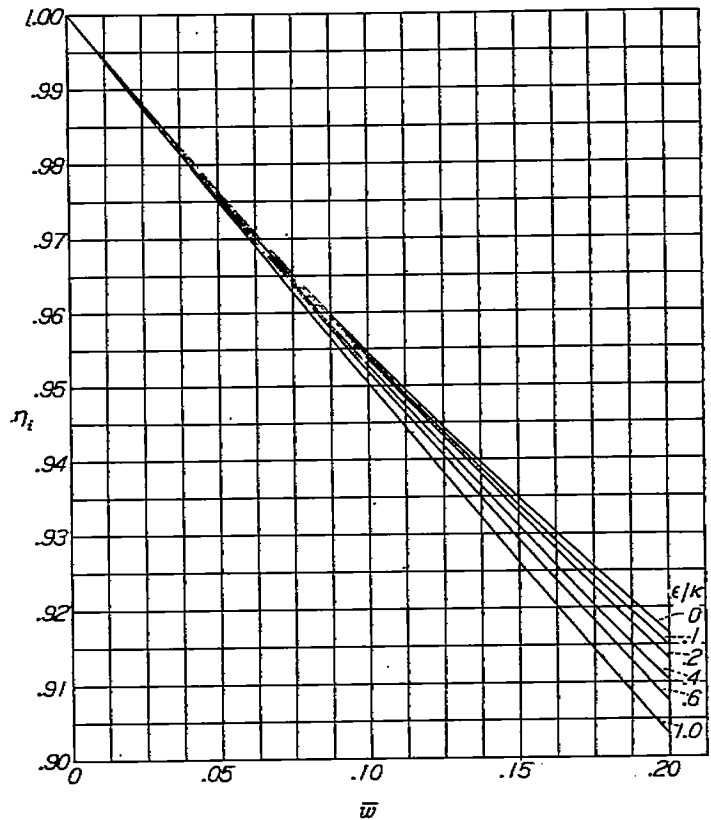


FIGURE 7.—Propeller efficiency against  $\bar{w}$  (reference 4).

and then use this value for the ideal coefficient

$$P_{c_T} \approx P_c = 2\kappa\bar{w}(1+\bar{w})\left(1 + \frac{\epsilon}{\kappa}\bar{w}\right)$$

to find  $\bar{w}$ .

It was shown in reference 4 that the dependence of the efficiency on  $\epsilon/\kappa$  in the efficiency formulas is very small and that it is sufficient to know only the approximate value of  $\epsilon/\kappa$ . An examination of the formulas for  $c_d$  and  $P_c$  shows that their dependence on  $\epsilon/\kappa$  is also small. It was further concluded in reference 4 that  $\epsilon/\kappa$  is only slightly greater than  $\kappa$  and that the practice of using  $\epsilon/\kappa$  instead of  $\kappa$  is considered satisfactory for design purposes. However, there appears to exist a simple relation between the axial-loss factor  $\epsilon$  and the total-loss factor  $\kappa$ . This relation takes on the form of a differential equation

$$\frac{\epsilon}{\kappa} = 1 + \frac{1}{2} \lambda \frac{d\kappa}{d\lambda}$$

where

$$\lambda = \frac{1}{\pi} \frac{V+w}{nD_0}$$

This relation has been checked and found to be exact for an infinite number of blades, and numerical checks for a two-blade propeller were in very close agreement. It is considered accurate for an empirical relation for design purposes for propellers of other numbers of blades.

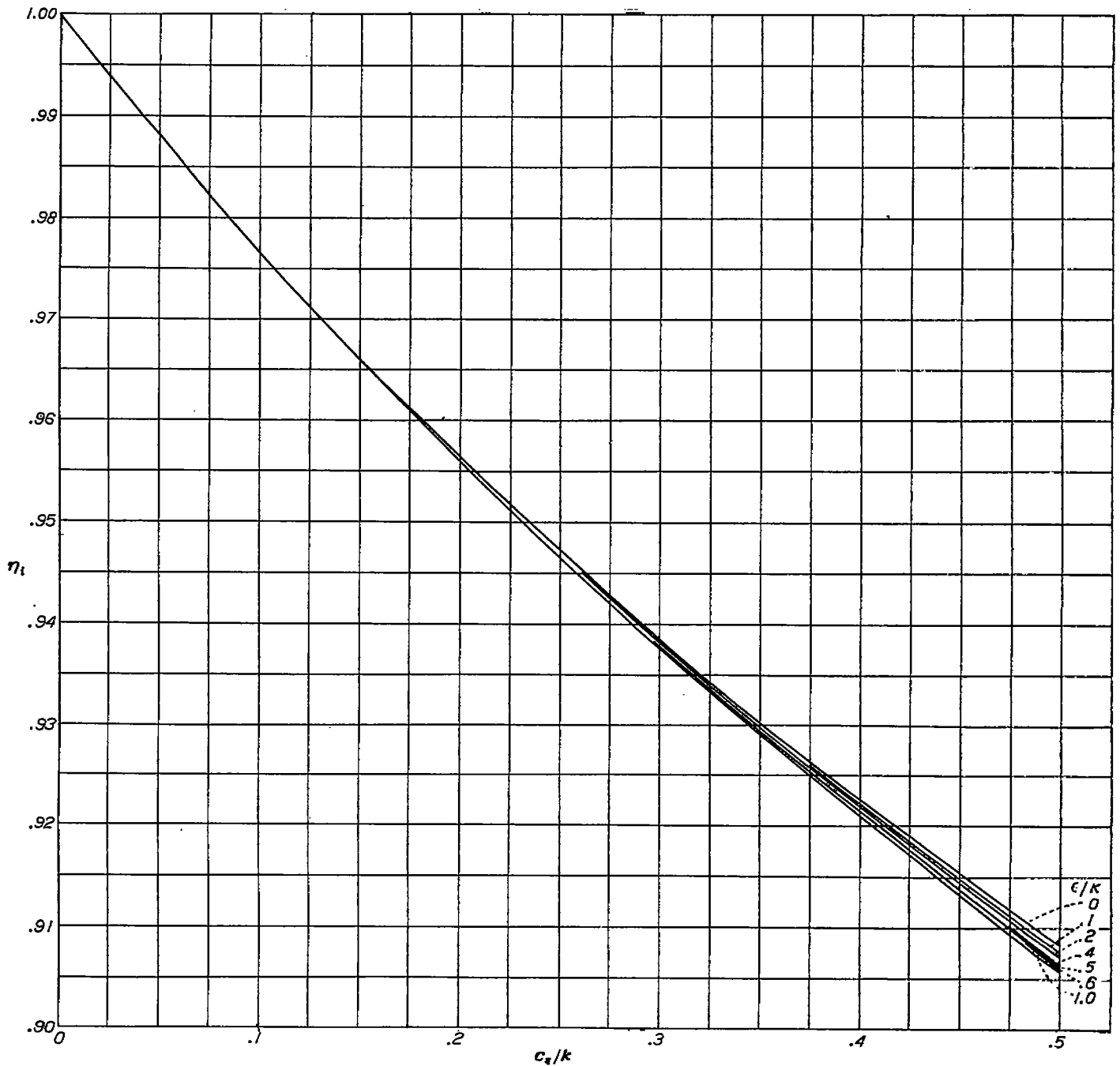


FIGURE 8.—Propeller efficiency against  $C_t/k$  (reference 4).

First obtain

$$\lambda_e = \frac{1}{\pi} \frac{V}{nD}$$

as a first approximation to  $\lambda$  for use in the calculations. Then read off  $\kappa$  and  $d\kappa/d\lambda$  from the appropriate charts of  $\kappa$  against  $\frac{V}{nD} (1 + \bar{w})$  for several values of  $\bar{w}$  (figs. 5 and 6).

Curves of  $\epsilon$ ,  $\kappa$ , and  $\epsilon/\kappa$  are plotted against  $\frac{V}{nD} (1 + \bar{w})$  in figures 10 and 11. Next plot a curve for the right side of the equation for  $P_c$  against  $\bar{w}$ . Where this curve intersects the horizontal line,  $P_c = P_{cT}$  is the desired point. This value may be checked from the chart by inserting the values obtained from the plot in the equation. Thus are obtained  $\kappa$ ,  $\bar{w}$ ,

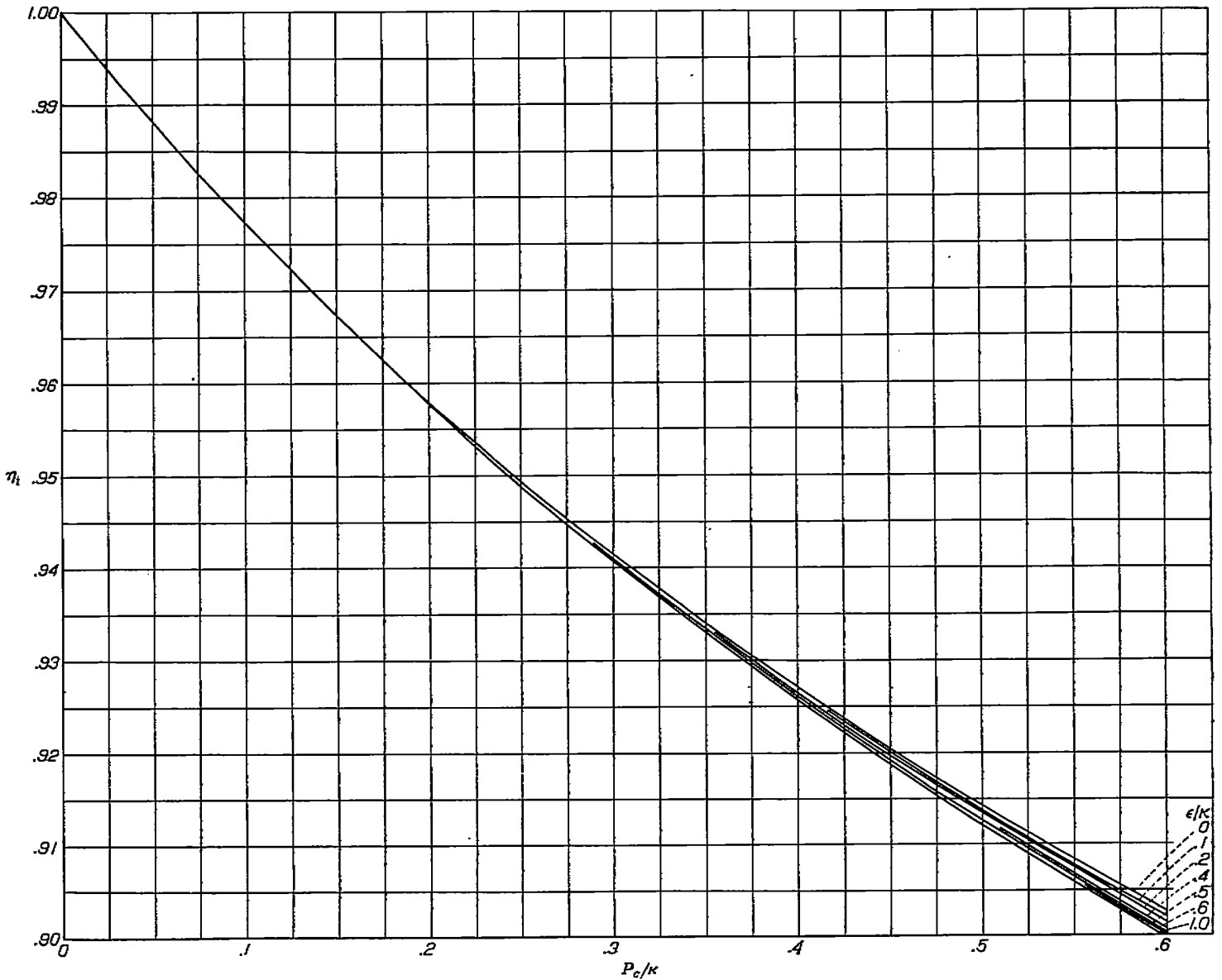


FIGURE 9.—Propeller efficiency against  $P_c/k$ .

$\frac{V}{nD} (1+\bar{w})$ , and  $\epsilon/k$ . From the chart of  $P_c/k$  (fig. 9), the optimum efficiency may be obtained.

The following examples illustrate the method of determining the optimum distribution of  $bc_i$  along the radius for both single-rotating and dual-rotating propellers that give the maximum possible efficiency (neglecting blade profile drag) that can be obtained with either propeller for one specified design condition.

ILLUSTRATIVE EXAMPLES

Single rotation.—Let the following data specify the propeller design conditions:

Power, horsepower.....	2,000
Density, slugs per cubic foot.....	0.001065
Velocity, miles per hour.....	425

The propeller selection has been made to the extent that the following data specify the propeller:

Rotational speed, $n$ , revolutions per second.....	23
Propeller diameter, $D$ , feet.....	12
Number of blades, $B$ .....	4
$V/nD$ .....	2.258

The total  $P_{cT}$  from the given conditions is

$$P_{cT} = \frac{P}{\frac{1}{2}\rho V^3 \pi R^2}$$

$$= \frac{(2000)(550)}{\frac{1}{2}(0.001065)(623)^3 \pi (6)^2} = 0.075$$

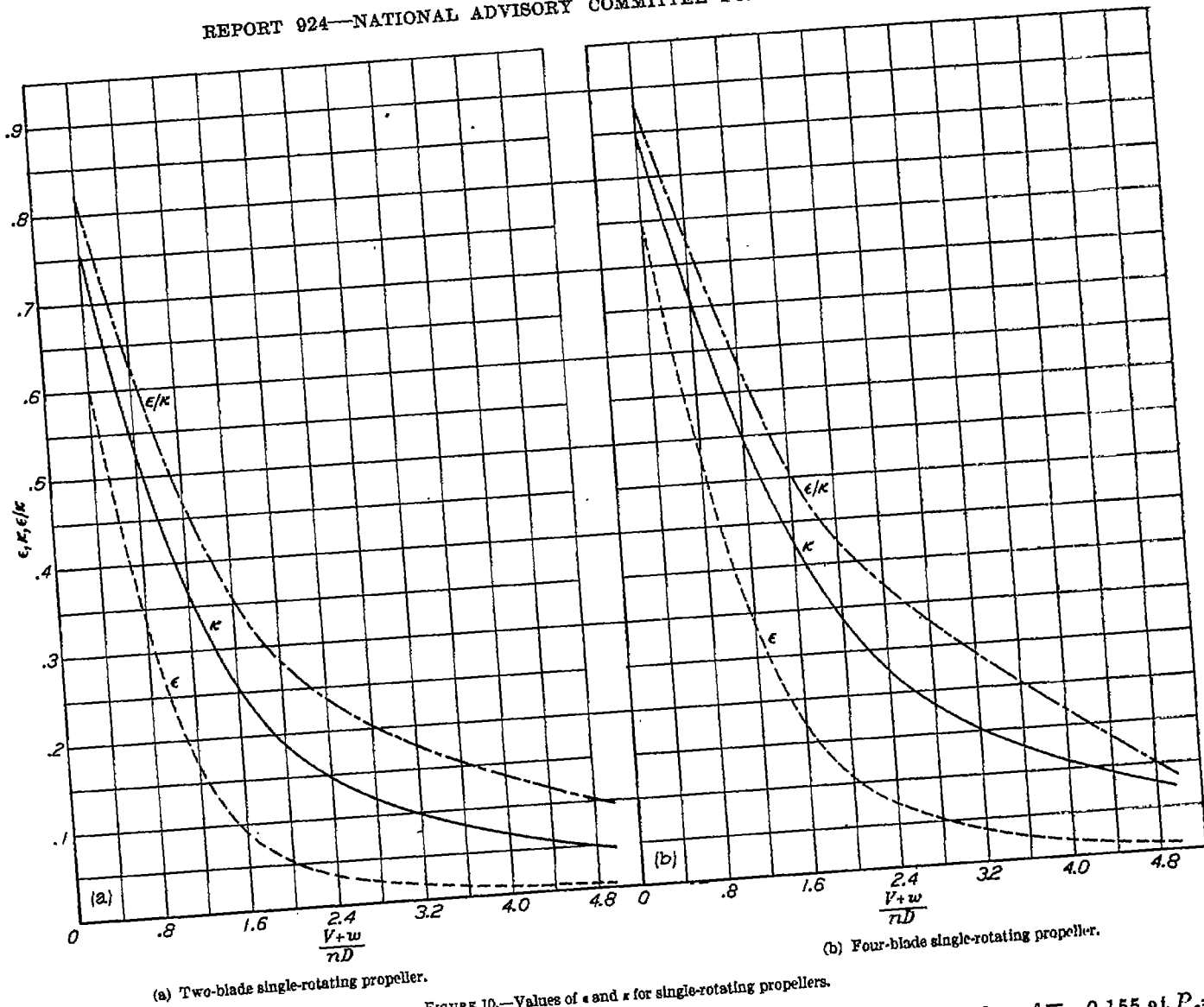


FIGURE 10.—Values of  $\epsilon$  and  $\kappa$  for single-rotating propellers.

The value of  $P_c$  should be based on the wake diameter  $D_0$  instead of on the propeller diameter  $D$  and should be used to calculate  $\bar{w}$ . Both  $P_c$  and the contraction may be obtained by successive approximations but the two effects tend to cancel each other and generally  $P_{cT}$  based on the propeller diameter is sufficiently accurate to use in the calculation of  $\bar{w}$ . The relation between  $\bar{w}$  and  $P_c$  is given by equation (16) as

$$P_c = 2\kappa\bar{w}(1+\bar{w}) \left(1 + \frac{\epsilon}{\kappa}\bar{w}\right)$$

where

$$P_c = P_{cT}$$

If values of  $\bar{w}$  are selected to cover the range and the curve for the four-blade propeller in figure 10 (b) is used, the following table is obtained for the four-blade single-rotating propeller:

$\bar{w}$ (assumed)	$\kappa$	$\epsilon/\kappa$	$P_c$
0	0.245	0.340	0
.1	.215	.318	.0488
.2	.191	.299	.0970

A plot of  $P_c$  against  $\bar{w}$  gives a value of  $\bar{w}=0.155$  at  $P_c=0.075$ . Then,

$$\frac{V}{nD}(1+\bar{w}) = (2.258)(1.155) = 2.81$$

From figure 10 (b),  $\kappa$  is read at  $\frac{V}{nD}(1+\bar{w})=2.61$ , and the optimum propeller efficiency  $\eta_i$  for a four-blade single-rotating propeller is read from figure 9. Thus

$$\kappa = 0.201$$

$$\frac{P_c}{\kappa} = 0.373$$

and

$$\eta_i = 0.929$$

With  $\bar{w}$  determined,  $\sigma c_i$  for the single-rotating propeller may be found by a direct calculation from equation (6)

$$\sigma c_i = \frac{1+w}{\left(1 + \frac{1}{2}\bar{w}\right) \left(1 + \frac{1}{2}\bar{w} \cos^2\phi\right)} \frac{2\bar{w}K(x) \frac{\sin^2\phi}{\cos\phi}}{\cos\phi}$$

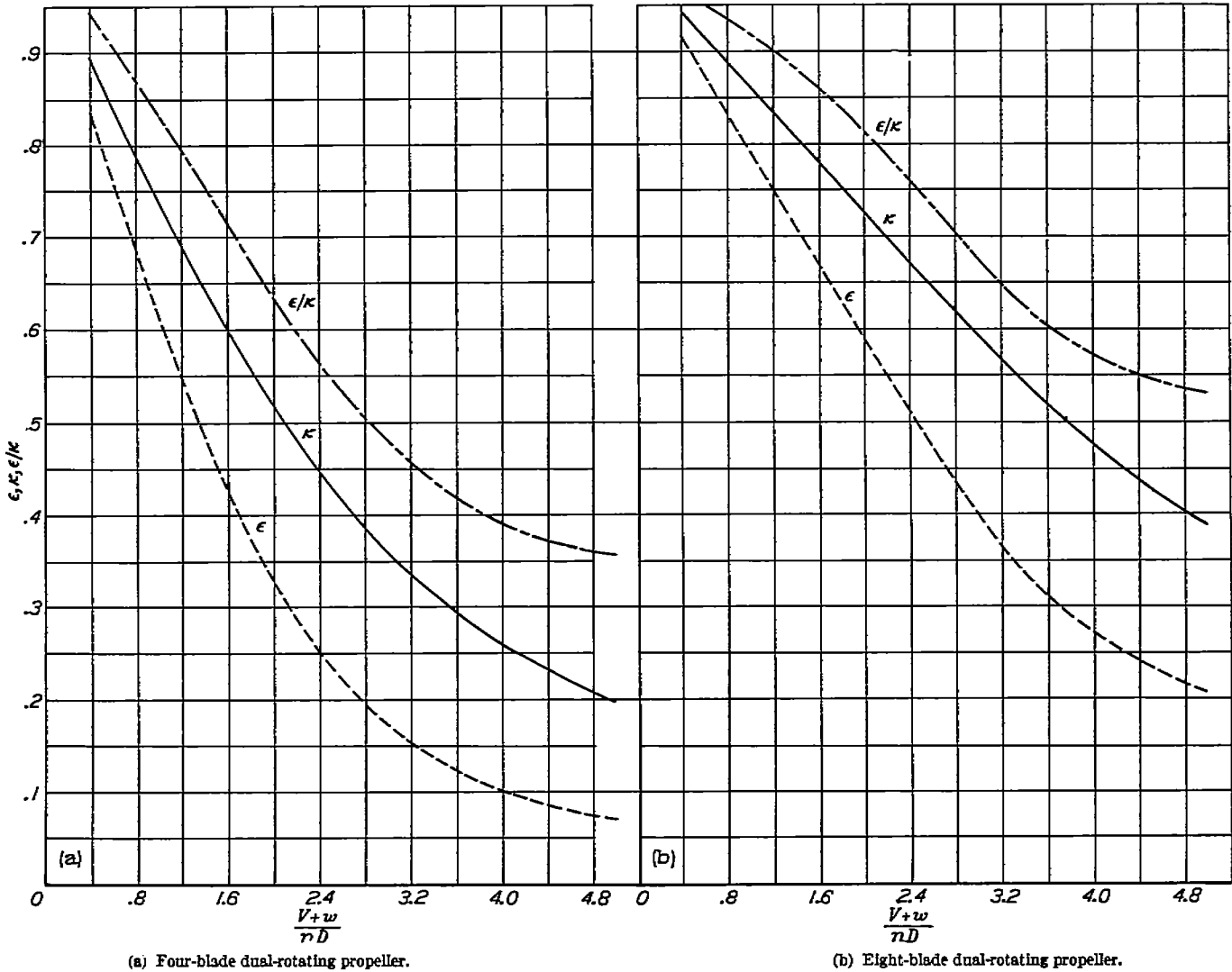


FIGURE 11.—Values of  $\epsilon$  and  $\kappa$  for dual-rotating propellers.

Values of the circulation function  $K(x)$  at each station are obtained from figure 3 (b) at  $\frac{V}{nD}(1+\bar{w})=2.61$  and the angle of the relative velocity at the propeller is given for each station by

$$\tan \phi = \frac{1}{\pi nD} \frac{V}{x} \left( 1 + \frac{1}{2} \bar{w} \right)$$

Performing these calculations for  $\bar{w}=0.155$  gives the values of  $\sigma c_i$  and  $b c_i$  in the following table (the blade-width distribution, in feet, for a constant  $c_i$  of 0.5 is also given):

$x$	$\tan \phi$	$K(x)$	$\sigma c_i$	$b c_i$	$b$ (ft)	$\frac{b c_i}{(b c_i)_{0.7R}}$
0.1	7.74	0.033	0.0842	0.079	0.158	0.167
.2	3.870	.078	.0967	.182	.364	.386
.3	2.580	.133	.1054	.298	.596	.631
.4	1.935	.185	.1044	.393	.786	.833
.5	1.548	.225	.0952	.449	.898	.92
.6	1.280	.260	.0855	.483	.966	1.023
.7	1.106	.271	.0716	.472	.944	1.000
.8	.968	.267	.0564	.417	.834	.880
.9	.860	.254	.0394	.309	.618	.655
.95	.815	.246	.0241	.216	.432	.458

Dual rotation.—The procedure is repeated for a 12-foot-diameter four-blade dual-rotating propeller for the same design conditions as used for the single-rotating propeller. The following table is obtained for the four-blade dual-rotating propeller (values of  $\kappa$  and  $\epsilon/\kappa$  were found from figure 11 (a)):

$\bar{w}$	$\kappa$	$\epsilon/\kappa$	$P_c$
0	0.472	0.589	0
.1	.432	.547	.1002
.2	.398	.519	.211

In this case a plot of  $P_c$  against  $\bar{w}$  gives a value of  $\bar{w}=0.075$  at  $P_c=0.075$ . Therefore,

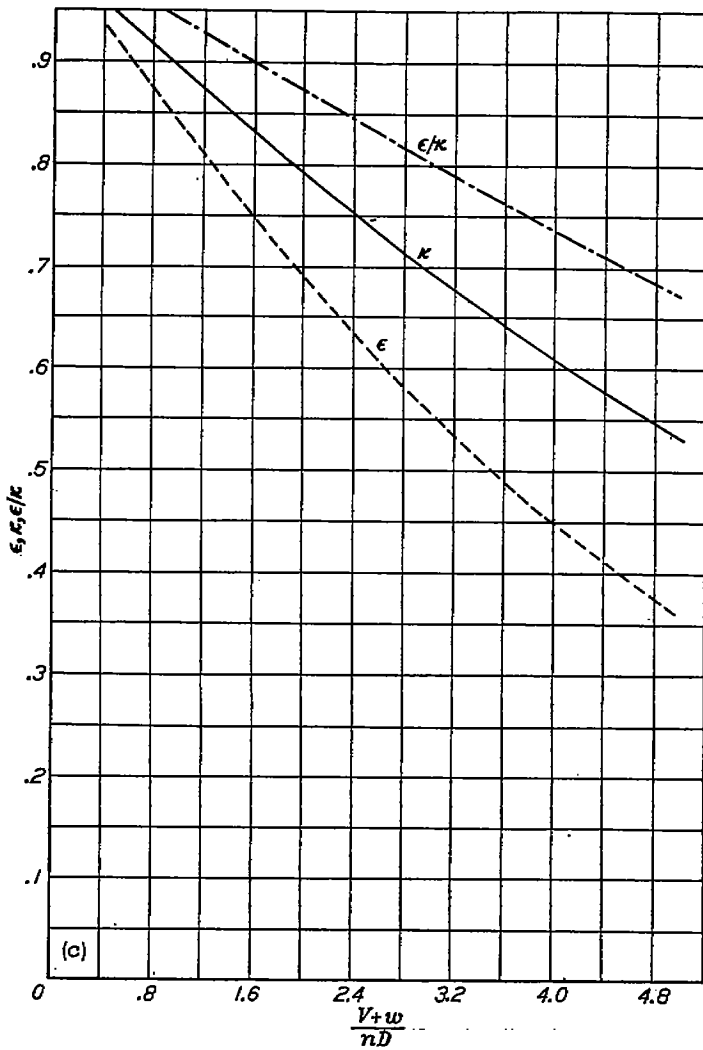
$$\frac{V}{nD}(1+\bar{w})=2.426$$

$$\kappa=0.442$$

$$\frac{P_c}{\kappa}=0.170$$

and

$$\eta_i=0.964$$



(c) Twelve-blade dual-rotating propeller.

FIGURE 11.—Concluded.

It is seen that the important parameter, the mass-flow coefficient, is 0.442 for the dual-rotating propeller and is only 0.201 for the single-rotating propeller. The efficiency (without drag) is 96.4 percent for the dual-rotating propeller but is only 92.9 percent for the single-rotating propeller.

For the dual-rotating propeller the values of  $\sigma c_i$  may be found for the front component from equation (12); thus,

$$(\sigma c_i)_F = \frac{V}{nD} \frac{1}{\pi x} \frac{(1+\bar{w})\bar{w} \sin \phi_0}{1 + \frac{1}{4} \kappa \bar{w} \sin^2 \phi_0} K(x)$$

and for the rear propeller from equation (13)

$$(\sigma c_i)_R = \frac{V}{nD} \frac{1}{\pi x} \frac{(1+\bar{w})\bar{w} \sin \phi_0}{1 + \frac{3}{4} \kappa \bar{w} \sin^2 \phi_0} K(x)$$

Equation (9) gives  $\phi_F$  by

$$\tan \phi_F = \frac{V}{nD} \frac{1}{\pi x} \left[ 1 + \frac{1}{2} \bar{w} \left( 1 + \frac{1}{2} \kappa \tan^2 \phi \right) \right]$$

and  $\phi_R$  is given in equation (11) by

$$\tan \phi_R = \frac{V}{nD} \frac{1}{\pi x} \left[ 1 + \frac{1}{2} \bar{w} \left( 1 - \frac{1}{2} \kappa \tan^2 \phi \right) \right]$$

Values of the circulation function  $K(x)$  are obtained from figure 4 (a) at the appropriate value of  $\frac{V+w}{nD} = \frac{V}{nD} (1+\bar{w})$ . Performing these calculations for  $V=623$ ,  $n=23$ ,  $D=12$ ,  $\bar{w}=0.075$ , and  $\kappa=0.442$  gives the values of  $\tan \phi$  and  $\sigma c_i$  in the following table:

$x$	$K(x)$	$\tan \phi_F$	$\tan \phi_R$	$(\sigma c_i)_F$	$(\sigma c_i)_R$	$(bc_i)_F$	$(bc_i)_R$
0.1	0.620	10.768	4.146	0.3510	0.3400	0.064	0.054
.3	.607	2.608	2.363	.1069	.1058	.624	.618
.4	.596	1.916	1.812	.0745	.0738	.564	.556
.5	.572	1.618	1.466	.0532	.0526	.501	.496
.6	.535	1.258	1.227	.0373	.0369	.422	.418
.7	.486	1.075	1.056	.0286	.0285	.378	.376
.8	.417	.939	.926	.0200	.0199	.302	.301
.9	.317	.833	.824	.0126	.0126	.214	.214
.95	.241	.789	.781	.0088	.0088	.167	.157

A comparison of the optimum distribution of  $bc_i$  along the blade for the dual-rotating propeller from this table with the optimum distribution for the single-rotating propeller as given in the preceding section shows that, if approximately constant  $c_i$  is absorbed along the blade, wide differences in blade plan form will result for the two propellers designed for the same operating condition. For the operating conditions selected, the maximum  $bc_i$  for the single-rotating propeller occurs near the 0.6 radius and tapers rapidly toward the tip and the hub, being only slightly over 16 percent of its maximum value at the 0.1 radius. On the other hand, the minimum value of  $bc_i$  for optimum distribution for the dual-rotating propeller occurs at the propeller tip and progressively increases toward the inner radii. The value of  $bc_i$  at the 0.1 radius is four times its value at the 0.95 radius.

Since the design of the dual-rotating propeller calls for high loading over the inner sections, the efficiency of the dual-rotating propeller is less susceptible to compressibility losses which normally occur near the propeller tip for operation at high tip Mach numbers. The compressibility losses may be reduced by reducing the width of these sections or by reducing the operating lift coefficient.

**Effect of blade drag on efficiency.**—The loss in efficiency due to the profile drag of the blades can be calculated from equations (20) to (22) if the blade-width distribution and profile-drag coefficients at the operating  $c_i$  are known. Inasmuch as structural requirements may determine the shape of the blade, especially over the inner radii, only one example is given. The equations, however, may be applied to any plan form. The example selected is for the four-blade single-rotating propeller on which the induced efficiency has been previously calculated. The shank sections of the propeller blade were assumed to be round, similar to the Hamilton Standard Propeller No. 3155-6 and the blade plan form from  $x=0.3$  to  $x=1.0$  was made optimum for a  $c_i$  of 0.5. The profile-drag coefficients for the several radii are



the same as given in reference 7 for the Hamilton Standard Propeller No. 3155-6 which has Clark Y sections and are given in the following table. It is assumed that a spinner covers the inner 0.2 of the radius. The distribution of  $\sigma c_t$  with  $x$  and of  $\sin \phi$  with  $x$  have been included in the table:

$x$	$\sigma c_t$	$\sigma$	$c_d$	$\sin \phi$	$\frac{\sigma c_d}{\sin \phi} x$	$\frac{\sigma c_d}{\sin \phi} x^2$
0.2	0.0967	0.1934	0.400	0.988	0.01600	0.00064
.3	.1054	.2108	.100	.932	.00897	.00061
.4	.1044	.2088	.020	.839	.00188	.00030
.5	.0932	.1904	.010	.840	.00113	.00028
.6	.0855	.1710	.008	.790	.00104	.00037
.7	.0716	.1432	.007	.742	.00085	.00046
.8	.0554	.1108	.006	.696	.00077	.00049
.9	.0364	.0728	.006	.652	.00060	.00049

Performing the integrations and substituting in the formulas gives for rotational-drag-loss coefficient

$$t_r = \frac{2}{\lambda_s^2} \int_{0.2}^{1.0} \frac{\sigma c_d}{\sin \phi} x^3 dx$$

$$= \frac{2}{0.516} (0.000348) = 0.0014$$

and for the axial-drag-loss coefficient

$$t_a = 2 \int_{0.2}^{1.0} \frac{\sigma c_d}{\sin \phi} x dx$$

$$= 2(0.00213) = 0.0043$$

The induced thrust coefficient has been given by equation (14) as

$$c_s = 2\kappa \bar{w} \left[ 1 + \bar{w} \left( \frac{1}{2} + \frac{\epsilon}{\kappa} \right) \right]$$

$$= 2(0.201)(0.155) \left[ 1 + 0.155 \left( \frac{1}{2} + 0.29 \right) \right] = 0.0700$$

and the induced power coefficient by equation (16) as

$$P_c = 2\kappa \bar{w} (1 + \bar{w}) \left( 1 + \frac{\epsilon}{\kappa} \bar{w} \right)$$

$$= 2(0.201)(0.155)(1.155)(1.045) = 0.0754$$

The induced efficiency is

$$\eta_i = \frac{c_s}{P_c}$$

$$= \frac{0.0700}{0.0754} = 0.929$$

With drag included, the total thrust is given by

$$c_{sT} = c_s - t_a$$

$$= 0.0700 - 0.0043 = 0.0657$$

and

$$P_{cT} = P_c + t_r$$

$$= 0.0754 + 0.0014 = 0.0768$$

The efficiency is

$$\eta = \frac{c_{sT}}{P_{cT}} = \frac{0.0657}{0.0768} = 0.855$$

Thus it is seen that the blade drag of the magnitude given in the preceding table reduces the propeller efficiency from 92.9 percent to 85.5 percent for the propeller operating conditions given.

#### CONCLUDING REMARKS

A comparison of Theodorsen's propeller theory with the conventional vortex theory shows that the optimum load distribution along the blade for single-rotating propellers obtained by the two theories is essentially identical and as a result the optimum efficiencies are the same for a given operating condition. Theodorsen's theory has the advantage, however, that the optimum efficiency for any design condition can be obtained quickly and accurately by the use of the mass coefficient  $\kappa$  without any laborious calculations and before the final design is made.

The distribution of the circulation function  $K(x)$  for the idealized dual-rotating propeller is radically different from the existing values for the single-rotating propeller that have been previously used for the dual-rotating propeller. Also, the mass coefficient  $\kappa$  for the dual-rotating propeller is larger than the sum of the values for two single-rotating propellers. These quantities, which are not available from mathematical computations but are obtained from the electrical-analogy method of Theodorsen, are used herein for obtaining the optimum load distribution along the blade for the dual-rotating propeller.

LANGLEY AERONAUTICAL LABORATORY,  
NATIONAL ADVISORY COMMITTEE FOR AERONAUTICS,  
LANGLEY FIELD, VA., March 15, 1948.

#### REFERENCES

1. Theodorsen, Theodore: The Theory of Propellers. I—Determination of the Circulation Function and the Mass Coefficient for Dual-Rotating Propellers. NACA Rep. 775, 1944.
2. Theodorsen, Theodore: The Theory of Propellers. II—Method for Calculating the Axial Interference Velocity. NACA Rep. 776, 1944.
3. Theodorsen, Theodore: The Theory of Propellers. III—The Slipstream Contraction with Numerical Values for Two-Blade and Four-Blade Propellers. NACA Rep. 777, 1944.
4. Theodorsen, Theodore: The Theory of Propellers. IV—Thrust, Energy, and Efficiency Formulas for Single- and Dual-Rotating Propellers with Ideal Circulation Distribution. NACA Rep. 778, 1944.
5. Goldstein, Sydney: On the Vortex Theory of Screw Propellers. Proc. Roy. Soc. (London), ser. A, vol. 123, no. 792, April 6, 1929, pp. 440-465.
6. Lock, C. N. H., and Yeatman, D.: Tables for Use in an Improved Method of Airscrew Strip Theory Calculation. R. & M. No. 1674, British A.R.C., 1935.
7. Crigler, John L., and Talkin, Herbert W.: Charts for Determining Propeller Efficiency. NACA ACR L4129, 1944.
8. Glauert, H.: Airplane Propellers. The Vortex Theory. Vol. IV of Aerodynamic Theory, div. L, ch. VI, sec. 1, W. F. Durand, ed., Julius Springer (Berlin), 1935, p. 231.